

# Thermal Characteristics of Surface Fire Spreading Front Under Ambient Wind

Ziwei Wang<sup>1, a</sup>, Kuibin Zhou<sup>1, b, \*</sup>, Xianzheng Ma<sup>1, c</sup> and Mengxing Li<sup>1, d</sup>

<sup>1</sup> College of Safety Science and Engineering, Nanjing Tech University, Nanjing, Jiangsu 211816, China.

<sup>a</sup> 1471701407@qq.com, <sup>b</sup> kbzhou@njtech.edu.cn, <sup>c</sup> 1098574991@qq.com, <sup>d</sup> 2873780029@qq.com

**Abstract.** Surface fire is the most common form of forest fire, primarily spreading along the forest land's surface and causing damage to nearby low-lying seedlings, shrubs, and the root systems of vegetation at its base. In actual forest fire scenarios, the occurrence of fires is often accompanied by environmental winds due to the typically complex terrain in forested areas. Forest vegetation is densely distributed, and when surface fires encounter obstacles such as tree trunks, the advancing fire front may interact with the tree trunks under the influence of environmental winds. This study focuses on understanding the thermal characteristics of the interaction between the advancing fire front and tree trunks in the presence of environmental winds. To investigate this interaction, temperature measurements are conducted on both sides of the obstacles and in the downstream region of the flame. Additionally, measurements of radiant heat flux are taken in the upper space above the experimental setup. By analyzing flame morphology parameters and experimental measurements, trends in thermal characteristic parameters with spatial position are identified. Regression formulas are developed to describe the temperature difference between the windward and leeward sides of the obstacles and the height above the experimental platform. Furthermore, the influence of flame climbing on radiant heat transfer in the upper space is discussed.

**Keywords:** Surface fire; Ambient wind; Standing leeward flame; Thermal radiation.

## 1. Introduction

The surface fire that occurs in forests can spread continuously, primarily because the high temperature of the fire front radiates energy towards the unburned materials ahead, increasing their temperature until they reach the ignition point and ignite. Consequently, the radiant heat transfer from the surface fire front to the ground downstream plays a crucial role in determining the rate of forest fire spread and the extent of damage. Previous studies have extensively investigated various aspects of surface fire spread, including flame spread rate, flame temperature, radiation and convective heat transfer from the flame to the unburned materials downstream, as well as flame geometry characteristics [1-7]. However, there is currently a relatively limited amount of research on the heat transfer effects of surface fire interacting with vegetation.

To address this gap, Tunstall et al. [8] conducted a study where they constructed four cylinders of different diameters and placed 24 thermocouples at four directions and six heights. Their aim was to understand the heat distribution around tree trunks during fire incidents. They discovered that the maximum temperature occurred at a height of 40 cm above the ground on the leeward side of the cylinder. Another study by Gutsell et al. [9] explained observations related to the formation of tree burn scars based on fluid dynamics and heat transfer processes. They found that as the fire passed through the trunk, the height of the flame increased on the lee side of the tree due to the appearance of two lee vortices. The suppression of turbulent mixing between fuel and air caused the flame height within the vortices to increase. Conceição et al. [10] developed a numerical model to calculate changes in temperature distribution on tree trunks when affected by the spread of fire. The simulated calculations showed temperatures exceeding the tolerance limit of the trees, resulting in the death of the trunk tissue located in the first layer beneath the trunk surface. Ju et al. [11] conducted experimental measurements on the downstream radiation and convective heating of methane and propane gas flames under crosswind conditions. The experimental measurements indicated that, under the same external conditions, the radiant heat flux of propane flames was

slightly higher than that of methane flames, while the convective heat flux exhibited the opposite trend. Wan et al. [12] performed a thermal radiation measurement experiment involving two identical pool fires in still air. By altering the size and distance of the burner, they measured the radiant heat flux at a distance above the vertical flame. They proposed a new weighted multi-point source model, which accurately predicts the radiant heat flux at the target point when deviating from the center line of the two-cell fire, in comparison to the single-point source model. Ren et al. [13] conducted experimental studies investigating the downstream heating and flow dynamics induced by flames on inclined surfaces. The experimental results demonstrated that when the surface slope angle reached  $18^\circ$ , flame-wall attachment phenomena began to occur, regardless of the fireline intensity. Previous researchers have extensively studied the thermal properties of flames; however, these studies did not consider the interaction between spreading flames and downstream obstacles.

In this paper, the thermal characteristics of surface fire spreading front interacting with tree trunk under ambient wind are studied. The temperature distribution of the downstream wall of the flame and the radiant heat flux of the target are measured experimentally. In addition, the longitudinal temperature distribution on the windward side and the leeward side of the obstacle and the radiant heat flux of the target position above the flame receiving the climbing flame on the leeward side of the obstacle are also measured. Finally, according to the flame shape parameters and experimental measurement results, the variation trend of thermal characteristics parameters with spatial position is summarized. The fitting formula of the temperature difference between the windward and leeward sides of obstacles and the height above the test platform is established. The effect of flame climbing on the radiant heat transfer in the upper space is also discussed. In order to improve the study of the climbing behavior of the surface fire spreading front.

## 2. Experimental

The experimental setup, as shown in Figure 1, is designed to measure the temperature and radiant heat flux interactions between the advancing surface fire front and tree trunks. Thermocouples are represented by solid dots in the main view (Figure 1 (a)). A total of 15 thermocouples are utilized, with 5 measuring the temperature on the downstream wall of the burner and 10 on both the windward and leeward sides of the obstacle. The distance between the burner and the first thermocouple downstream ( $L_d$ ) is 10 cm, while the distance between the bottom thermocouples on both sides of the obstacles and the experimental table surface ( $L_u$ ) is also 10 cm. The thermocouples are positioned at a 10 cm interval downstream of the burner and on either side of the obstacle. The thermocouple measuring the wall temperature downstream of the burner is in close contact with the experimental table surface, with the working end distributed along the downstream centerline. The thermocouples on both sides of the obstacles are positioned on the centerline of their windward and leeward faces. Solid rectangles in the figure represent radiant heat flux meters located downstream of the burner, while hollow rectangles represent heat flux meters situated above the burner. The heat flux meter downstream of the burner is used to measure the radiant heat flux from the flame to the downstream wall, and its arrangement is the same as that of the thermocouples. The heat flux meter above the burner is employed to measure the radiant heat flux from the climbing flame to the upper space (i.e., the tree canopy in realistic scenarios). The first heat flux meter is positioned at a distance  $L_{ud}$  of 7.5 cm from the obstacles, and the distance between the two heat flux meters at this location is also 7.5 cm. A plan view of the measurement setup is provided in Figure 1 (b).

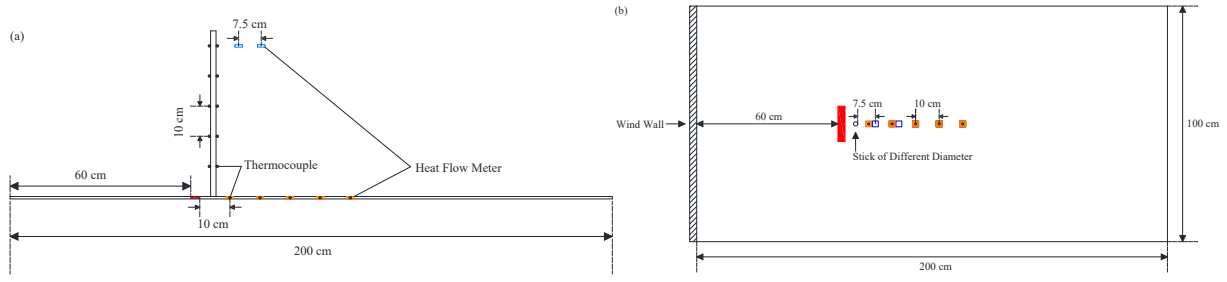


Fig. 1 Experimental device for measuring temperature and radiant heat flux (a) front view, (b) vertical view

To compare the differences in flame temperature and radiant heat flux between flame climbing phenomena occurring and not occurring, this study selected an obstacle with a diameter of  $d = 1.8$  cm and set two typical distances,  $D = 2.1$  cm and  $D = 5.4$  cm, between the obstacles and the burner corresponding to flame climbing and no flame climbing phenomena under this diameter. Two fireline intensities are selected, respectively  $\dot{Q}_l = 46.36$  kW/m and  $\dot{Q}_l = 83.46$  kW/m. The effective wind speed is selected as  $U_e = 0.53$  m/s and  $U_e = 1.10$  m/s, respectively, as shown in Table 1.

Table 1. The test conditions of thermal characteristic measurement experiment

$d$ (cm)	$D$ (cm)	$U_e$ (m/s)	$\dot{Q}_l$ (kW/m)	$L_d$ (cm)	$L_u$ (cm)	$L_{ud}$ (cm)
1.8	2.1	0.53	46.36	10	10	7.5
	5.4	1.10	83.46	20	20	15
				30	30	
				40	40	
				50	50	

### 3. Results and discussion

#### 3.1 Temperature distribution on the downstream wall

The experimental measurement results of the downstream wall temperature of the burner are shown in Figure 2. Figure 2 (a) shows the variation of the downstream wall temperature,  $T_d$ , with time for a spacing of 2.1 cm between the obstacle and the burner, a fireline intensity of 46.36 kW/m, and an effective wind speed of 1.10 m/s. The data values collected every 5 seconds are highlighted. As shown, it can be observed that the downstream wall temperature remains smoothly with time, and the temperature decreases as the distance between the measurement point and the burner increases. When the distance to the burner is relatively close ( $L_d \leq 30$  cm), the temperature at different measurement points is vary significantly due to the influence of the flame length ( $L_x$ ). However, when the distance to the burner is greater ( $L_d \geq 40$  cm), since the measurement points are primarily located outside  $L_x$ , the difference between the wall temperature and the ambient temperature is significantly reduced.

Figure 2 (b) shows the variation of the wall temperature ( $T_d$ ), with  $L_d$  for different operating conditions. The two conditions  $D = 2.1$  cm and  $D = 5.4$  cm correspond to the occurrence and non-occurrence of flame ascent, respectively. It can be found that under the same conditions, when  $L_d$  is larger, the wall temperature without flame climb is slightly higher compared to the case with flame climb. The reason is that the  $L_x$  decreases when the flame climbs, which weakens the heat transfer effect on the downstream wall, resulting in a slight decrease in its temperature. In addition, the wall temperature also increases with the increase of fireline intensity and effective wind speed under the same conditions.

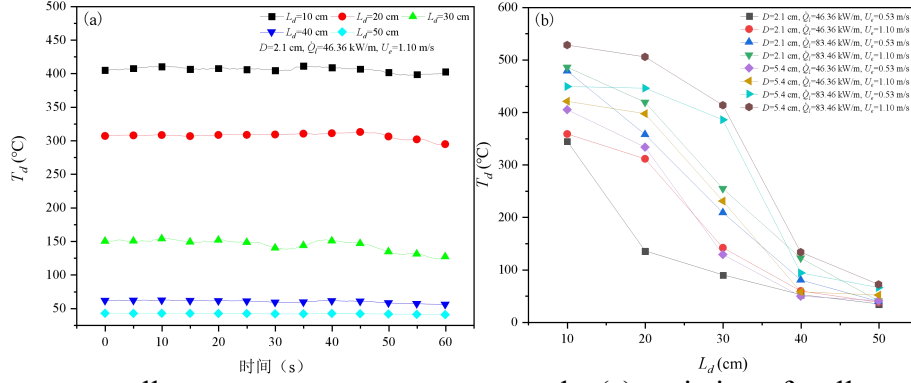


Fig. 2 Downstream wall temperature measurement results (a) variation of wall temperature with time (b) variation of wall temperature with the downstream distance of the burner

### 3.2 Temperature distribution on both sides of the obstacle

When the flame climbing phenomenon occurs, the longitudinal climbing flame will appear on the leeward side of the obstacle, which will cause significant temperature difference between the leeward side and the windward side of the obstacle. Figure 3 (a) and (b) respectively show the variation of temperature difference ( $\Delta T$ ) between the leeward and windward sides of the obstacle with the height above the experimental platform for flame ascent and non-ascent scenarios. It can be observed that when flame climbing occurs, there is a significant temperature difference between the two sides of the obstacle over a large height range. When  $L_u$  is greater than 30 cm, the measurement points are beyond the flame climbing height range, and the temperature difference between the two sides gradually decreases. However, for the scenario without flame climbing, except for the measurement point closest to the surface of the experimental platform, there is no significant temperature difference between the two sides of the obstacle at higher positions. The temperature difference at  $L_u = 10$  cm may be due to its proximity to the flame, resulting in a higher temperature on the leeward side of the obstacle. However, the magnitude of this temperature difference is much smaller compared to the temperature difference caused by flame climbing, as shown in Figure 3 (a).

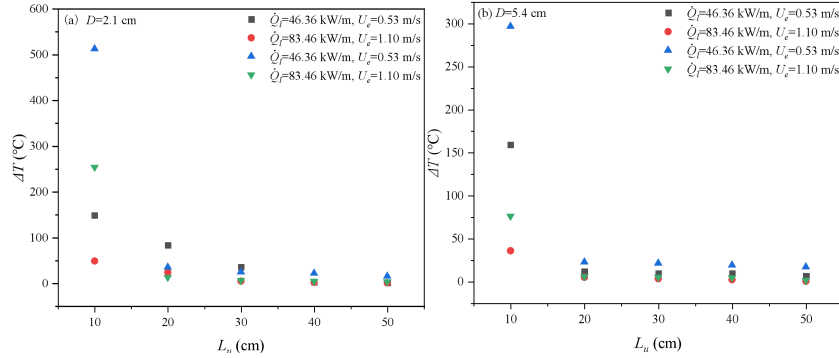


Fig. 3 Variation of temperature difference on both sides of the obstacle with the height above the experimental platform (a) with occurrence of standing leeward flame ( $D = 2.1$  cm) (b) no occurrence of standing leeward flame ( $D = 5.4$  cm)

In this paper, this study uses the height of flame ascent on the leeward side of the obstacle ( $H_{SLF}$ ) to nondimensionalize the height above the experimental platform, considering the relative size of flame climbing height and height above the platform. When the temperature difference on both sides of the obstacle and the nondimensionalized height are substituted into the equation, the results are shown in Figure 4. It presents a power function relation and satisfies as following:

$$\Delta T = 41.16(L_u / H_{SLF})^{-2.26} \quad (1)$$

Where,  $L_u / H_{SLF}$  is the dimensionless height above the experimental platform.

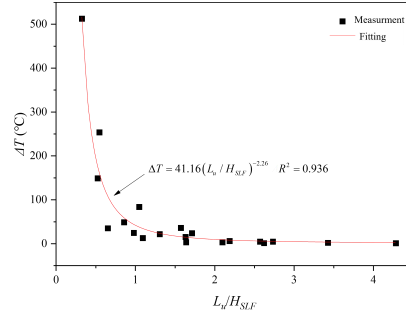


Fig. 4 Quantitative relationship between the temperature difference on both sides of the obstacle and the dimensionless height

### 3.3 Heat flux distribution on downstream wall

Figure 5 shows the measurement results of the heat flux at different positions on the downstream wall of the burner when the fireline intensity is 46.36 kW/m, and the effective wind speed is 0.53 m/s. As shown, the flame exhibits fluctuating behavior influenced by environmental airflow and its own buoyancy, causing the radiant heat flux on the downstream wall to fluctuate above and below the mean value. Under the same conditions, the radiant heat flux of the downstream wall decreases with the increase of the distance. When the measurement position is beyond the flame attachment length, the distance between the flame and the heat flux sensor increases rapidly, resulting in a significant decrease in the measured radiant heat flux. It is worth noting that when the measurement position is far from the burner, the heat flux sensor is located outside the horizontal flame length. It receives the minimum radiant heat flux, and the numerical fluctuations are relatively small.

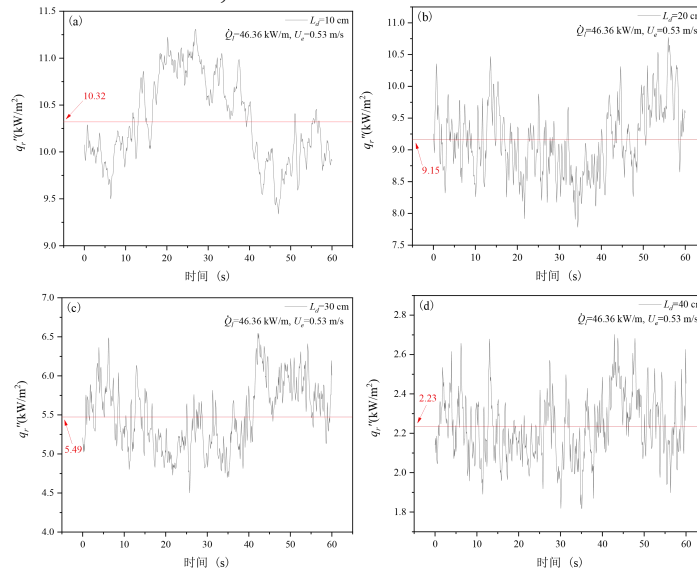


Fig. 5 Measurement results of radiant heat flux density at different positions downstream

Figure 6 illustrates the variation of radiant heat flux density with downstream distance ( $L_d$ ) under different operating conditions. The two conditions in the figure,  $D = 2.1$  cm and  $D = 5.4$  cm, correspond to the occurrence and non-occurrence of flame climbing phenomena, respectively. Similar to the trend of downstream wall temperature, radiant heat flux decreases with increasing downstream distance. The main difference between the two is the downstream distance at which a rapid decrease in numerical value occurs. The downstream wall temperature is primarily influenced by the horizontal flame length ( $L_x$ ), where the temperature significantly decreases beyond  $L_d \geq 30$  cm. On the other hand, the radiant heat flux on the downstream wall is mainly affected by the flame attachment length ( $L_a$ ). Under other identical conditions,  $L_a$  usually differs from  $L_x$  by 10 - 15 cm. Therefore, from the observation of Figure 6, it can be concluded that except for conditions with higher fireline intensity and effective wind speed, which exhibit larger  $L_a$ , the radiant heat flux for other conditions starts to decrease noticeably at  $L_d \geq 20$  cm.

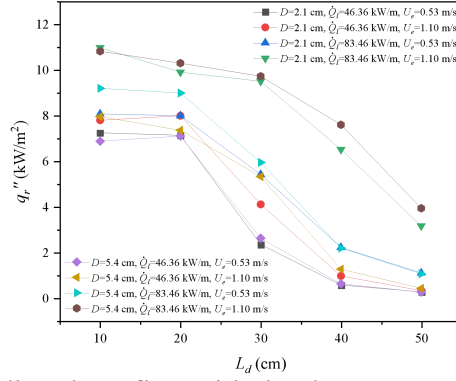


Fig. 6 Variation of radiant heat flux with the downstream distance of the burner

The effect of flame climbing on the downstream wall radiant heat flux is similar to that of wall temperature. For the downstream distances ( $L_d \geq 40$  cm), the flame climbing phenomenon affects  $L_a$  and  $L_x$  by affecting the downstream flame volume of the obstacle, which slightly reduces the radiant heat flux when the flame climbing phenomenon occurs.

### 3.4 Heat flux distribution on downstream wall

Figure 7 shows the radiant heat flux received by the two measurement points in the upper part of the flame. It can be seen, the variation in radiant heat flux in the upper part of the flame is related to whether the flame climbing phenomenon occurs. In the case of no flame climbing ( $D = 5.4$  cm), under other identical conditions, the values increase with increasing fireline intensity but decrease with increasing effective wind speed. When flame climbing phenomena occur ( $D = 2.1$  cm), the measurement point closer to the obstacle receives slightly higher radiant heat flux due to the shorter distance from the climbing flame.

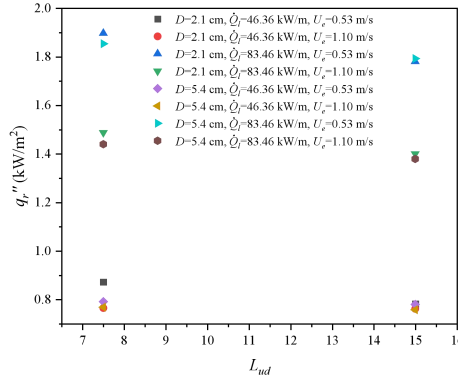


Fig. 7 Radiant heat flux received by the measuring point above the flame

## 4. Conclusion

This paper presents experimental measurements of wall temperature and radiant heat flux on the downstream wall of the flame, the temperature difference on the windward and leeward sides of the obstacle, and the radiant heat flux at the target position above the flame. A comparison is made between the thermal characteristics on the downstream wall in cases where flame climbing phenomena occur and where they do not, revealing differences. Additionally, measurements of the temperature difference and radiant heat flux on both sides of the obstacle are conducted during instances of flame climbing phenomena. The main research findings are as follows:

(1) The temperature and radiant heat flux on the downstream wall of the flame decrease with increasing distance, and under other identical conditions, they increase with increasing fireline intensity and effective wind speed. The occurrence of flame climbing phenomena affects the flame volume downstream of obstacles, resulting in slightly lower temperature and heat flux compared to their non-occurrence. Due to the different flame morphology parameters that predominantly affect

wall temperature and radiant heat flux, significant numerical changes occur at different downstream positions.

(2) The temperature difference on the windward and leeward sides of the obstacle is measured during instances of flame climbing phenomena. It is found that this difference decreases with increasing height above the experimental platform surface. By using the flame climb height for non-dimensional processing of the height above the experimental platform, a power function relationship between the temperature difference and the non-dimensional height is established, along with the corresponding fitting formula.

(3) The radiant heat flux received at two measurement points above the flame is compared for the occurrence and non-occurrence of flame climbing phenomena. Both measurements generally increase with increasing fireline intensity but decrease with increasing effective wind speed. In the case of flame climbing phenomena, the measurement point closer to the obstacle exhibits higher values, and with increasing effective wind speed, as the flame height decreases, the difference between the two measurement values also decreases.

## Acknowledgements

This work was supported by the National Natural Science Foundation of China under Grant nos. 51876088 and 51506082. KZ acknowledges the support from the Six Talent Peaks Project of Jiangsu Province of China under Grant no. XNYQC-005.

## References

- [1] Finney M A, Grumstrup T P, Grenfell I. Flame Characteristics Adjacent to a Stationary Line Fire. *Combustion Science and Technology*, 2020: 1-21.
- [2] Himoto K, Deguchi Y. Temperature elevation and trajectory in the downwind region of rectangular fire sources in cross-winds. *Fire Safety Journal*, 2020, 116.
- [3] Gong C, Ding L, Wan H, et al. Spatial temperature distribution of rectangular n-heptane pool fires with different aspect ratios and heat fluxes received by adjacent horizontal targets. *Fire Safety Journal*, 2020, 112.
- [4] Morvan D, Porterie B, Loraud J C, et al. A Numerical Investigation of Cross Wind Effects on a Turbulent Buoyant Diffusion Flame. *Combustion Science and Technology*, 2001, 164(1): 1-35.
- [5] Linn R R. Numerical simulations of grass fires using a coupled atmosphere–fire model: Basic fire behavior and dependence on wind speed. *Journal of Geophysical Research*, 2005, 110(D13).
- [6] Huang X, Wang Y, Zhu H, et al. Experimental study on the radiant heat flux of wall-attached fire plume generated by rectangular sources. *International Journal of Thermal Sciences*, 2021, 159.
- [7] Morvan D, Dupuy J L. Modeling of fire spread through a forest fuel bed using a multiphase formulation. *Combustion and Flame*, 2001, 127(1): 1981-1994.
- [8] Tunstall B, Walker J, Gill A. Temperature Distribution Around Synthetic Trees During Grass Fires. *Forest Science*, 1976, 22(3): 269-276.
- [9] Gutsell S L, Johnson E A. How fire scars are formed: Coupling a disturbance process to its ecological effect. *Can J Forest Res*, 1996, 26(2): 166-174.
- [10] Conceição E, Gomes J, Lúcio M M, et al. Numerical Evaluation of the Temperature Distribution in a Tree Trunk in a Forest Fire Environment. *Sustainable Development of Water and Environment: Proceedings of the ICSDWE2021*. Springer. 2021: 85-94.
- [11] Ju X, Gollner M J, Wang Y, et al. Downstream radiative and convective heating from methane and propane fires with cross wind. *Combustion and Flame*, 2019, 204: 1-12.
- [12] Wan H, Gao Z, Ji J, et al. Experimental study on flame radiant heat flux from two heptane storage pools and its application to estimating safety distance. *Energy*, 2019, 182: 11-20.
- [13] Ren X, Sluder E T, Heck M V, et al. Scaling analysis of downstream heating and flow dynamics of fires over an inclined surface. *Combustion and Flame*, 2022, 242.